actuators

MDPI

Article

Finite-Time Prescribed Performance Neural Network Force Control of Electro-Hydraulic Proportional Load Simulator with Output Feedback

Zhenle Dong [1,*], Chao Li [2], Pengxiang Zhang [1], Yilong Jia [1], Jianyong Yao [3] and Long Liu [4]

[1] School of Vehicle and Transportation Engineering, Henan University of Science and Technology, Luoyang 471000, China; 240320030371@stu.haust.edu.cn (P.Z.); 250320030440@stu.haust.edu.cn (Y.J.)
[2] Luoyang Aviation Office, Luoyang 471000, China; zhaolongchao0407@163.com
[3] School of Mechanical Engineering, Nanjing University of Science and Technology, Nanjing 210094, China; jerryyao.buaa@gmail.com
[4] No.650 Institute, AVIC Hongdu Aviation Industry Group, Nanchang 448001, China; liulong_njust@163.com
* Correspondence: dong_zhenle@163.com; Tel.: +86-133-8379-8719

Abstract

This paper focus on the high accuracy force control of electro-hydraulic proportional load simulator (EHPLS). Firstly, to weaken the influence of the unknown dead zone of the proportional valve, a mathematic model with a smooth inverse dead zone was constructed. Then, finite-time prescribed performance function, of which the desired steady-state value can be achieved within finite time, is defined to impose constraints on the tracking error, while the neural network feedback is introduced to compensate for the unknown dynamic, which can ensure the tracking accuracy further improved for the entire tracking process in the presence of unknown dead-zone parameters, unknown system parameters and disturbance. Finally, through design modification, the proposed control technologies are realized based on the output feedback signal. Comparative simulations under two desired force trajectories are carried out to verify the effectiveness of the proposed controller.

Keywords: load simulator; electro-hydraulic proportional system; finite-time prescribed performance control; output feedback; neural network

1. Introduction

Load simulator is mainly used to reproduce the demand load with high precision, and thanks to the advantages of high power-to-weight ratio and strong anti-load rigidity, a hydraulic load simulator has been widely employed in national defense and industry, such as an aerodynamic load simulation in missile ground testing [1], material tensile/compressive performance testing [2], mechanical structure resistance performance testing [3], etc. Due to the high cost-effective and superior anti-pollution ability, the proportional valve as the core control component has been welcomed more and more by designers and users [4]. Therefore, there is an urgent need for excellent controllers of electro-hydraulic proportional load simulators (EHPLS).

However, the hydraulic system has many inherent nonlinear behaviors, parametric uncertainties caused by different working conditions and temperatures, and unknown dynamics that are difficult to accurately model, which bring great difficulties to the development of control strategies. In view of this, researchers have also put forward many control methods, such as adaptive control [5], active disturbance rejection control [6], robust integral of the sign of the error [7], neural network control [8,9], etc. In addition,

Check for updates

Academic Editor: Ioan Ursu

Received: 24 December 2025
Revised: 30 January 2026
Accepted: 16 February 2026
Published: 4 March 2026

Copyright: © 2026 by the authors. Licensee MDPI, Basel, Switzerland. This article is an open access article distributed under the terms and conditions of the Creative Commons Attribution (CC BY) license.

the working mode of the load simulator makes it possible to face the motion disturbance caused by the movement or deformation from the loaded object; however, when static loading is implemented, that is, the test object is fixed in a certain position, to ensure the dynamic tracking accuracy of the output force is also a key performance index. This paper focuses on the tracking control of EHPLS under static loading. Static loading can validate the control performance of equipment in the absence of motion disturbances [10], and additionally evaluates the mechanical properties of materials or structural components under static forces.

In addition to the control difficulties mentioned above, the input nonlinearity of the proportional valve, especially the unknown dead zone at its middle position, may also weaken the performance and even lead to system instability. It is no exaggeration to say that the unknown dead zone nonlinearity has become the key to limit the performance improvement to a certain extent, properly compensating for the unknown dead zone has practical significance and is also the focus of this paper. After investigation, the existing methods in the literature to reduce the effects of dead zone can be summarized into two types. One is to model the dead zone as a combination of control input multiplied by gain and disturbance-like term [11]. In this design, the disturbance-like term will be included in the lumped unmodeled dynamic, and various robust means are employed to suppress the unmodeled dynamic. However, the complexity of disturbance components will inevitably require excessive robust gain, which will lead to the potential risk of high gain feedback and may stimulate the unmodeled structural dynamics. In addition, the lack of targeted dead zone compensation also leads to the limited control accuracy. Another method to minimize the influence of dead zone is to construct an inverse model of the dead zone [12] and then incorporate effective compensation and adaptive design for unknown dead-zone parameters. Since the discontinuous dead-zone inverse model proposed in [13] may cause control chatting, a smooth continuous dead-zone inverse model is proposed in [14]. Refs. [15,16] has applied this method to the electro-hydraulic position system, while integrating the nonlinear robust technology proposed in [17] to realize high-precision asymptotic position tracking while effectively compensating the unknown dead zone.

However, there are still some problems needing further attention. Firstly, for the EHPLS, there is still a lack of targeted control methods that can properly compensate the unknown dead zone with online adaptive law. Then, it is necessary to emphasize that the above existing literature are all aimed at the control accuracy at steady stage and lack sufficient description of the control performance of the whole control cycle, especially in the transient stage. In fact, although we can incorporate the necessary parametric adaptation law when designing the controller, uncertain hydraulic system parameters and dead zone parameters will inevitably lead to large or even unpredictable control error in the initial operation stage, and only controllers with steady-stage accuracy described are clearly unable to cope with this obstacle. In [17], an ingenious control method that can improve transient performance, namely prescribed performance control, is proposed. It imposes constraints on the convergence speed and overshoot of the tracking error by defining a prescribed indicator function, and then constructs the conversion error as the drive signal of the controller to obtain the expected performance. The successful application of this wonderful method has been realized in the electro-mechanical system and hydraulic position servo system. Subsequently, other derivative methods have also been developed, such as finite-time prescribed performance [18] and flexible prescribed performance [19], etc. However, for the electro-hydraulic proportional load simulator with an unknown dead zone, how to improve the control performance by applying the prescribed performance description has not been involved, and it is also worth studying. Finally, the above control methods all rely on full state feedback. In fact, considering the cost and installation space,

in many cases, the load simulator may only be equipped with a force sensor, and it is unrealistic to obtain all state signals at this time.

Motivated by the above analysis, this paper aims to fully improve the tracking accuracy of the EHPLS. First, by constructing a smooth inverse dead-zone model and adaptive estimations of the unknown dead-zone parameters; the influence of the unknown dead zone at middle position of the proportional valve is weakened. Then, the finite-time prescribed performance function, of which the desired steady-state value can be achieved within a finite time, is constructed to impose constraints on the tracking error, while the adaptive neural network control is utilized to compensate for the unknown dynamic and further improve the tracking performance in the presence of parametric uncertainties and disturbance. Finally, through design modification, the above technologies are realized based on output feedback signal.

The remainder of this paper is organized as follows: the mathematic model and transformation are presented in Section 2. Section 3 presents the detailed derivation process of finite-time prescribed performance control with neural network. Section 4 presents the controller redesign based on output feedback. Section 5 presents the verification of the proposed controller. The final section includes a conclusion and future research plan.

2. Mathematic Model and Transformation

2.1. Mathematics Model Considering the Valve Dead Zone

The EHPLS under consideration is illustrated in Figure 1, where a proportional valve is used to control a single-rod hydraulic linear cylinder. The loaded object is chosen as a hydraulic actuator. The goal is to have the load simulator to track any specified force trajectory as closely as possible.

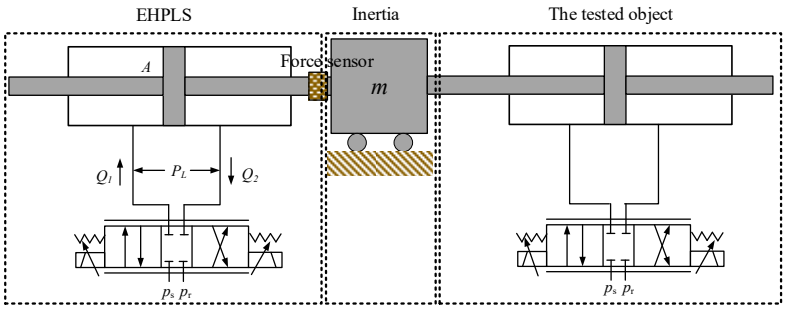


Figure 1. The schematic diagram of EHPLS.

The force output of the load simulator can be expressed as:

$$F = P_{\mathrm{L}} A + d_{\mathrm{f}}(t) \tag{1}$$

where F denotes force output, P_{L} denotes load pressure between the two chambers of the double-rod linear actuator, A denotes the effective area of linear actuator, and d_{f}(t) denotes the disturbance and other hard-to-model dynamic.

Due to the fact that the static loading is considered in the research, the actuator velocity is zero. The pressure flow equation can be expressed as

$$\frac{V_{\mathrm{t}}}{4\beta_{\mathrm{e}}} \dot{P}_{\mathrm{L}} = Q_{\mathrm{L}} - q_{\mathrm{L}} \tag{2}$$

where V_{t} denotes the total control volume of actuator, β_{e} denotes the effective bulk modulus, $Q_{\mathrm{L}} = (Q_1 + Q_2)/2$ is the load flow rate supplied by the proportional valve, Q_1 and Q_2 denote

the flow rate into and out of the hydraulic cylinder, and q_L denotes internal leakage of actuator and can be modeled as the quadratic polynomial form [10] of load pressure P_L, i.e.,

$$q_L = C_1 P_L^2 + C_2 P_L + C_3 \tag{3}$$

where C_1, C_2, C_3 are unknown constants and denote the internal leakage coefficients.

The load flow rate Q_L provided by the proportional valve is related to the valve spool displacement, i.e.,

$$Q_L = k_v x_v \sqrt{P_s - \text{sign}(x_v) P_L} \tag{4}$$

where $k_v = C_d w \sqrt{1/\rho}$ denotes the valve discharge gain and C_d is the discharge coefficient, w is the spool valve area gradient, ρ is the density of hydraulic oil, x_v denotes the valve spool displacement, P_s denotes the system supply pressure, and sign(•) is the standard sign function.

Neglecting the valve dynamics and considering the dead zone at the middle position of proportional valve, valve spool displacement x_v can be modeled as the nonlinear mapping of valve control voltage as

$$x_v(u) = \begin{cases} \kappa_1 u - \kappa_1 dz_1 & \text{if } u \geq dz_1 \\ 0 & \text{if } dz_2 < u < dz_1 \\ \kappa_2 u - \kappa_2 dz_2 & \text{if } u \leq dz_2 \end{cases} \tag{5}$$

where $\kappa_1 > 0$, $\kappa_2 > 0$, $dz_1 \geq 0$, $dz_2 \leq 0$ denote the right slope, left slope, right break-point and left break-point of the dead zone, respectively and these parameters are unknown constants. Equation (5) describes the dead-zone property of proportional valve and its graphical representation is shown in Figure 2a [15].

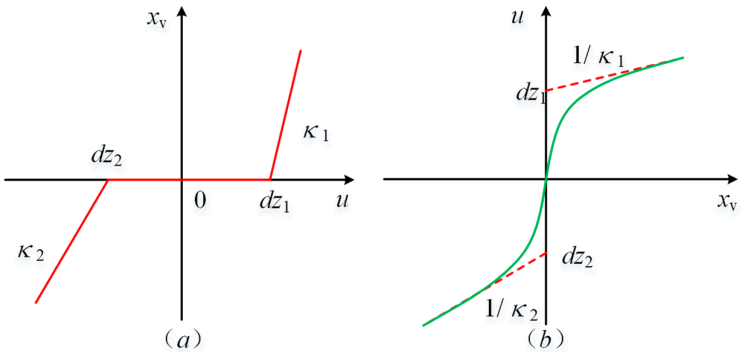


Figure 2. (**a**) Dead zone; (**b**) Smooth dead-zone inverse.

2.2. Model Transformation Based on Dead-Zone Inverse

As is clear from Equation (5), the dead-zone characteristic of the proportional valve is discontinuous, which makes the model-based compensation structure design difficult. Therefore, it is necessary to transform the system model to facilitate the subsequent controller design. Then, we try to introduce a smooth dead-zone inverse function proposed in [1], whose graphical expression is shown in Figure 2b. Define $DI(\bullet)$ to represent the smooth dead-zone inverse function, which can be expressed as

$$u = DI(x_v) = \frac{x_v + \kappa_1 dz_1}{\kappa_1} \chi_1(x_v) + \frac{x_v + \kappa_2 dz_2}{\kappa_2} \chi_2(x_v) \tag{6}$$

where $\chi_1(\bullet)$ and $\chi_2(\bullet)$ are smooth functions defined as

$$\chi_1(\bullet) = \frac{e^{\bullet/\varepsilon}}{e^{\bullet/\varepsilon} + e^{-\bullet/\varepsilon}} \quad , \quad \chi_2(\bullet) = \frac{e^{-\bullet/\varepsilon}}{e^{\bullet/\varepsilon} + e^{-\bullet/\varepsilon}} \tag{7}$$

where ε is a positive constant to be chosen.

Let $\boldsymbol{\vartheta} = [\vartheta_1, \vartheta_2, \vartheta_3, \vartheta_4]^{\mathrm{T}}$ denote the unknown dead-zone parameter vector, where $\vartheta_1 = \kappa_1$, $\vartheta_2 = \kappa_1 dz_1$, $\vartheta_3 = \kappa_2$, $\vartheta_4 = \kappa_2 dz_2$. Then, the dead-zone model given in Equation (5) can be linearly transformed to

$$x_{\mathrm{v}} = -\vartheta^T \eta \tag{8}$$

where $\eta = [-v_+ u, v_+, -v_- u, v_-]^{\mathrm{T}}$, and v_+, v_- are defined as

$$v_+ = \begin{cases} 1, & \text{if} \quad x_{\mathrm{v}} > 0 \\ 0, & \text{else} \end{cases}, \qquad v_- = \begin{cases} 1, & \text{if} \quad x_{\mathrm{v}} < 0 \\ 0, & \text{else} \end{cases} \tag{9}$$

It is clear that v_+ and v_- are discontinuous, which may cause inconvenience in the design of spool displacement x_{v}. Meanwhile, the dead-zone parameter ϑ is unknown, so we define

$$x_{\mathrm{vd}} = -\hat{\vartheta}^{\mathrm{T}} \widehat{\eta} \tag{10}$$

where $\hat{\vartheta} = [\hat{\vartheta}_1, \hat{\vartheta}_2, \hat{\vartheta}_3, \hat{\vartheta}_4]^{\mathrm{T}}$ denote the estimation of ϑ, and $\widehat{\eta} = [-\chi_1(u)u, \chi_1(u), -\chi_2(u)u, \chi_2(u)]^{\mathrm{T}}$.

Then we have

$$x_{\mathrm{v}} - x_{\mathrm{vd}} = -\vartheta^{\mathrm{T}}\eta + \hat{\vartheta}^{\mathrm{T}}\widehat{\eta} = -\vartheta^{\mathrm{T}}\widehat{\eta} + \vartheta^{\mathrm{T}}\widehat{\eta} - \vartheta^{\mathrm{T}}\eta + \hat{\vartheta}^{\mathrm{T}}\widehat{\eta} = \widetilde{\vartheta}^{\mathrm{T}}\widehat{\eta} + \vartheta^{\mathrm{T}}(\widehat{\eta} - \eta) \tag{11}$$

where $\widetilde{\vartheta} = \hat{\vartheta} - \vartheta$ denote the estimation deviation of ϑ.

Take the time derivation of Equation (1), and substitute Equations (2) and (4) into it, we have

$$\frac{V_{\mathrm{t}}}{4\beta_e k_{\mathrm{v}}}\dot{F} = x_{\mathrm{v}}\sqrt{P_{\mathrm{s}} - sign(x_{\mathrm{v}})P_{\mathrm{L}}} - \frac{C_1}{k_{\mathrm{v}}}P_L^2 - \frac{C_2}{k_{\mathrm{v}}}P_L - \frac{C_3}{k_{\mathrm{v}}} + \dot{d}_{\mathrm{f}}(t) \tag{12}$$

Then substitute Equations (2) and (4) into it

$$\theta_1 \dot{F} = g \cdot x_{vd} + \widetilde{\vartheta}^{\mathrm{T}}\widehat{\eta}\, g - \theta_2 P_{\mathrm{L}}^2 - \theta_3 P_{\mathrm{L}} - \theta_4 + \Delta \tag{13}$$

where $\theta_1 = V_{\mathrm{t}}/(4\beta_{\mathrm{e}}k_{\mathrm{v}})$, $\theta_2 = C_1/k_{\mathrm{v}}$, $\theta_3 = C_2/k_{\mathrm{v}}$, $\theta_4 = C_3/k_{\mathrm{v}}$ and

$$\begin{aligned} g &= \sqrt{P_{\mathrm{s}} - \mathrm{sign}(x_{\mathrm{v}})P_{\mathrm{L}}} \\ \Delta &= \dot{d}_{\mathrm{f}}(t) + \vartheta^{\mathrm{T}}\left(\widehat{\eta} - \eta\right)\sqrt{P_{\mathrm{s}} - \mathrm{sign}(x_{\mathrm{v}})P_{\mathrm{L}}} \triangleq F_{\mathrm{c}} + \widetilde{f} \end{aligned}$$

where F_{c} denotes the known continuous part of the lumped disturbance Δ, and $\widetilde{f}$ denotes the other disturbance.

Assumption 1: *the disturbance $\widetilde{f}$ and the unknown parameters θ_i, $i = 1, 2, 3, 4$ satisfy the following properties:*

$$\theta_{i\min} \le \theta_i \le \theta_{i\max} \quad , \qquad \widetilde{f} \le \varepsilon \tag{14}$$

where $\theta_{i\max}$, $\theta_{i\min}$ are known constants and denote the upper bound and lower bound of θ_i respectively, ε is an unknown constant.

Assumption 2: *the state x_1, x_2, P_1 and P_2 are available for measurement.*

The control objective of this research can be described as follows: given the desired force trajectory F_{d}, synthesize a control input u for EHPLS such that the actual force y tracks y_{d} as closely as possible.

https://doi.org/10.3390/act15030150

2.3. Controller Design

2.3.1. Finite-Time Prescribed Performance Function

Define the force tracking error $z = F - F_d$. Considering the high-precision control of the whole trajectory tracking stage, especially the complex transient stage that has always been ignored in the previous literature, we first plan the error z and assume that it meets

$$-\phi(t) < z(t) < \phi(t) \tag{15}$$

where $\phi(t)$ is a smooth decreasing positive function defined as [18,20,21]

$$\phi(t) = \begin{cases} \left(\phi_0 - \frac{t}{T_f}\right)\exp(1 - \frac{T_f}{T_f - t}) + \phi_\infty & t \in [0, T_f) \\ \phi_\infty & t \in [T_f, \infty] \end{cases} \tag{16}$$

where $\phi_0 > 0$, $\phi_\infty > 0$ denote adjustable parameters, T_f denotes the adjustable time. It is clear that the function $\phi(t)$ holds the following properties: (1) $\phi(t) > 0$; (2) $\dot{\phi}(t) < 0$; (3) $\lim_{t \to T_f} \phi(t) = \phi_\infty$, and for any $t \geq T_f$, $\phi(t) = \phi_\infty$. Therefore, it is easy to check that Equation (15) gives the finite-time prescribed performance description of tracking error z, where $-\phi(t)$ and $\phi(t)$ preset the maximum downward impulse and maximum overshoot on tracking error respectively, and ϕ_∞ preset the convergence region at steady stage, which can be achieved within a finite time.

2.3.2. Prescribed Performance Force Control with Dead-Zone Compensation and Neural Network

Define the design error ξ as

$$\xi = z/\phi(t) \tag{17}$$

It is clear from Equation (17) that the finite-time prescribed performance defined in Equation (15) and (16) can be achieved provided that $|\xi| < 1$ is guaranteed.

Define the following logarithmic barrier Lyapunov function

$$V_1 = \frac{\theta_1}{2}\ln\frac{1}{1 - \xi^2} \tag{18}$$

Taking the derivative of Equation (18), we have

$$\begin{aligned} \dot{V}_1 &= \frac{z(\theta_1\dot{F} - \theta_1\dot{F}_d - z_1\dot{P})}{\phi(1-\xi^2)} \\ &= \frac{\xi(g \cdot x_{vd} + \hat{\vartheta}^T\widehat{\eta}\, g - \theta_2 P_L^2 - \theta_3 P_L - \theta_4 + F_c + \widetilde{f} - \theta_1\dot{F}_d - \theta_1\xi\dot{\phi})}{\phi(1-\xi^2)} \end{aligned} \tag{19}$$

Noting Equation (19), the desired valve spool displacement x_{vd} can be designed as

$$\begin{aligned} x_{vd} &= (x_{vda} + x_{vds1} + x_{vds2})/g \\ x_{vda} &= \hat{\theta}_1(\dot{F}_d + \xi\dot{\phi}) + \hat{\theta}_2 P_L^2 + \hat{\theta}_3 P_L + \hat{\theta}_4 \\ x_{vds1} &= -k\xi - \frac{\xi}{\phi(1-\xi^2)} \end{aligned} \tag{20}$$

where x_{vda} is model-based compensation component, x_{vds1} is the linear stabilizing component, x_{vds2} is the NN term to be designed, k is positive adjustable gain, and $\hat{\theta}_i$ denotes the estimation of parameter θ_i, $i = 1, 2, 3, 4$.

From Equation (19), we can construct the NN approximation for unknown continuous function F_c, i.e.,

$$F_c = W^T\sigma(X) + \omega^* \tag{21}$$

where $W = [W_1, W_2, \ldots, W_q]^{\mathrm{T}}$ is the unknown ideal NN weight matrix, and q is the number of NN nodes in the hidden layer, $\sigma(X)$ is the activation function and X denotes the input vector, ω^* denotes the bounded NN approximate deviation.

$$x_{\mathrm{vds2}} = -\hat{F}_{\mathrm{c}} = -\hat{W}^{\mathrm{T}}\sigma(X) \tag{22}$$

where $\widetilde{W} = \hat{W} - W$ denote the estimation deviation of W, and the input vector for σ is chosen as $X = [1, F_{\mathrm{d}}, P_{\mathrm{L}}]^{\mathrm{T}}$.

Substituting Equations (20) and (22) into Equation (19), we have

$$\dot{V}_1 = -\frac{k\xi^2}{\phi(1-\xi^2)} + \frac{\widetilde{\vartheta}^{\mathrm{T}}\widehat{\eta}g + \widetilde{\theta}_1\varphi - \widetilde{W}^{\mathrm{T}}\sigma(X)}{\phi(1-\xi^2)} + \frac{\xi(\widetilde{f} - \omega^*)}{\phi(1-\xi^2)} - \frac{\xi^2}{\phi^2(1-\xi^2)^2} \tag{23}$$

where $\widetilde{\theta} = \hat{\theta} - \theta$ denote the estimation deviation of θ, $\theta = [\theta_1, \theta_2, \theta_3, \theta_4]^{\mathrm{T}}$, $\varphi = [(\dot{F}_{\mathrm{d}} + \xi\dot{\phi}), {P_{\mathrm{L}}}^2, P_{\mathrm{L}}, 1]^{\mathrm{T}}$ is the parametric regressor.

Then from Equation (6), the final control input for the load simulator can be calculated via

$$u = DI(x_{\mathrm{vd}}) = \frac{x_{\mathrm{vd}} + \hat{\vartheta}_2}{\hat{\vartheta}_1}\chi_1(x_{\mathrm{vd}}) + \frac{x_{\mathrm{vd}} + \hat{\vartheta}_4}{\hat{\vartheta}_3}\chi_2(x_{\mathrm{vd}}) \tag{24}$$

2.4. Main Results

Provided that the initial output force track error satisfies

$$-\phi(0) < z(0) < \phi(0) \tag{25}$$

where $\bar{\varepsilon}$ is positive constant, and the adaptive laws are designed as

$$\begin{aligned} &\dot{\hat{\theta}} = -\Gamma_\theta[\xi\varphi/\phi(1-\xi^2) - k_\theta\hat{\theta}], \quad \dot{\hat{\vartheta}} = -\Gamma_\vartheta[\xi\widehat{\eta}g/\phi(1-\xi^2) - k_\vartheta\hat{\vartheta}], \\ &\dot{\hat{W}} = \Gamma_W[\sigma(X)\xi/\phi(1-\xi^2) - k_W\hat{W}] \end{aligned} \tag{26}$$

where Γ_θ, Γ_ϑ, Γ_W are diagonal matrix of selectable parameters, $k_\theta > 0$, $k_\vartheta > 0$, $k_W > 0$ are selectable parameters. Then, the proposed controller Equations (20), (22) and (24) could guarantee that all signals in the whole EHPLS are bounded, that is, the system will always be stable, while the finite-time prescribed performance described in Equations (15) and (16) for force tracking error z will always hold.

Proof: see Appendix A.

3. Controller Redesign with Output Feedback

By analyzing the proposed controller given in Equations (20), (22) and (24), we can see its operation needs to collect not only the output force signal, but also the load pressure signal P_{L}. However, in most cases, considering the hardware cost and installation space constraints, the load simulator will not install expensive pressure sensors. In addition, the collection of pressure signals will inevitably introduce high-frequency noise, resulting in the quality of control input signals, and thus affecting the achievable load control accuracy. So in this section, we will consider the high-precision force control when the load simulator is not equipped with pressure sensors. At this time, the controller will only rely on the output force signal, therefore our task is to redesign the controller with output feedback.

From Equation (1), we can make the following approximation for static loading, i.e.,

$$P_L \approx P_F \tag{27}$$

where $P_{\mathrm{F}} = F/A$.

Then the output force dynamic Equation (12) can be rewritten as

$$\frac{V_t}{4\beta_e k_v}\dot{F} = x_v\sqrt{P_s - sign(x_v)P_F} - \frac{C_1}{k_v}P_F^2 - \frac{C_2}{k_v}P_F - \frac{C_3}{k_v} + \dot{d}(t) \tag{28}$$

Considering the dead-zone inverse, we have

$$\theta_1\dot{F} = g_F \cdot x_{vd} + \widetilde{\vartheta}^T\widehat{\eta}\, g - \theta_2 P_F^2 - \theta_3 P_F - \theta_4 + \Delta_F \tag{29}$$

where

$$\begin{aligned} g_F &= \sqrt{P_s - \mathrm{sign}(x_v)P_F} \\ \Delta_F &= \dot{d}(t) + \vartheta^T\left(\widehat{\eta} - \eta\right)\sqrt{P_s - \mathrm{sign}(x_v)P_F} + \widetilde{d} = F_{co} + \widetilde{f}_o \end{aligned}$$

where $\widetilde{d}$ denotes the approximation error caused by Equation (27), and F_{co} denotes the known continuous part of the lumped disturbance Δ_F, and $\widetilde{f}_o$ denotes the other disturbance. From Assumption 1 and the actual operating conditions of the load simulator, it can be inferred that Δ_F is still bounded, so we assume that $\widetilde{f}_o \le \varepsilon_o$, where ε_o is an unknown constant.

By referring to the derivation procedure of the earlier control design part, we can design the desired valve spool displacement x_{vd} with output feedback, i.e.,

$$\begin{aligned} x_{vd} &= (x_{vda} + x_{vds1} + x_{vds2})/g_F \\ x_{vda} &= \hat{\theta}_1(\dot{F}_d + \xi\dot{\phi}) + \hat{\theta}_2 P_F^2 + \hat{\theta}_3 P_F + \hat{\theta}_4 \\ x_{vds1} &= -k\xi - \tfrac{\xi}{\phi(1-\xi^2)} \\ x_{vds2} &= -\hat{W}^T\sigma(X) \end{aligned} \tag{30}$$

and the adaptive laws are designed as

$$\begin{aligned} &\dot{\hat{\theta}} = -\Gamma_\theta[\xi\varphi_F/\phi(1-\xi^2) - k_\theta\hat{\theta}],\ \dot{\hat{\vartheta}} = -\Gamma_\vartheta[\xi\widehat{\eta}\, g_F/\phi(1-\xi^2) - k_\vartheta\hat{\vartheta}], \\ &\dot{\hat{W}} = \Gamma_W[\sigma(X)\xi/\phi(1-\xi^2) - k_W\hat{W}] \end{aligned} \tag{31}$$

where $\varphi_F = [(\dot{F}_d + \xi\dot{\phi}), P_F^2, P_F, 1]^T$.

Eventually, the final control input u for the EHPLS can be calculated via Equation (24). Obviously, the operation of u depends only on the output force signal F.

As long as the conditions in Equation (25) are satisfied, the redesigned controller Equations (30) and (31) that only relies on the output force signal can still guarantee that all signals in the whole EHPLS are bounded, while the finite-time prescribed performance described in Equations (15) and (16) for force tracking error z will always hold.

The proof process is similar to Appendix A and will not be repeated here.

4. Controller Verification

The effectiveness of the proposed control algorithm for EHPLS has been verified based on the simulation, and the parameters of the system are listed in Table 1.

The values of C1, C2, and C3 are taken from our previous research [10].

To fully verify the performance of the proposed controller, the following three controllers are utilized for comparison:

(1) C1: This is the proposed finite-time prescribed performance output feedback force control with the neural network, and the detailed form is given in Equations (30) and (31). The controller parameters are chosen as follows: k = 40, ϕ_0 = 20, ϕ_∞ = 2, T_f = 1, $k_\theta = 1 \times 10^{-11}$, k_ϑ = 0.0025, ε = 0.0025, Γ_θ = diag [1×10^{-23}, 0.0001, 1×10^{-24}, 1×10^{-10}], Γ_ϑ= diag [0.01, 1×10^{-12}, 0.01, 1×10^{-5}]. The neural network parameters are chosen as q = 10, kw = 0.5, Va = 0.8, Γ_W = diag [0.85, 0.85, 0.85, 0.85].

(2) C2: This is the adaptive neural network force control without dead-zone compensation. The detailed controller form is

$$\begin{aligned} z &= F - F_{\mathrm{d}} \\ u &= (u_{\mathrm{a}} + u_{\mathrm{s}} + u_{\mathrm{NN}})/g \\ u_{\mathrm{a}} &= \hat{\theta}_1 \dot{F}_{\mathrm{d}} + \hat{\theta}_2 P_{\mathrm{L}}^2 + \hat{\theta}_3 P_{\mathrm{L}} + \hat{\theta}_4 \\ u_{\mathrm{s}} &= -kz\ ,\ \ u_{\mathrm{NN}} = -\hat{W}^{\mathrm{T}}\sigma(X)\ ,\ \ X = [1, F_d, P_L]^T \\ \dot{\hat{\theta}} &= -\Gamma_\theta[\varphi - k_\theta\hat{\theta}]\ ,\ \ \dot{\hat{W}} = \Gamma_W[\sigma(X) - k_W\hat{W}] \end{aligned} \tag{32}$$

The controller parameters are chosen as follows: k = 40, $k_\theta = 1 \times 10^{-4}$, k_ϑ = 0.025, ε = 0.0025, Γ_θ= diag [1×10^{-5}, 1×10^{-22}, 1×10^{-11}, 1], Γ_ϑ = diag [0.01, 0.1, 0.01, 0.01]. The neural network parameters are chosen as q = 10, kw = 2.5×10^{-8}, Va = 3×10^{-8}, Γ_W = diag [20, 20, 20, 20].

(3) C3: This is the widely applied proportional-integral controller. The controller parameters are chosen as follows: k_{p} = 0.022, k_{i} = 0.01.

Table 1. Specifications of the EHPLS.

Parameters	Symbol	Values	Units
Hydraulic system parameters	A	9.05×10^{-4}	m^2
	β_{e}	200×10^6	Pa
	k_{v}	2.394×10^{-8}	$\mathrm{m}^4/(\mathrm{s}\cdot\mathrm{V}\cdot\mathrm{N}^{-1/2})$
	P_{s}	7×10^6	Pa
	V_{t}	7.96×10^{-5}	m^3
	P_{r}	0	Pa
	C_1	-7.6852×10^{-20}	$\mathrm{m}^7/(\mathrm{N}^2\cdot\mathrm{s})$
	C_2	2.7594×10^{-12}	$\mathrm{m}^5/(\mathrm{N}\cdot\mathrm{s})$
	C_3	-2×10^{-5}	m^3/s
Dead-zone parameters	dz_1	0.1	V
	dz_2	0.1	V
	κ_1	1	
	κ_2	1	

4.1. Case 1

The desired trajectory is selected as a sine-like command F_{m} = 4000 arctan(sin (0.5πt)) $(1 - \exp(-0.5t^3))/0.7854$ N. The initial system force is set to 0 N. The simulation duration is 30s with a step size of 0.2 ms.

The tracking performance of C1 is shown in Figure 3. The error comparison among all controllers is presented in Figure 4. Analysis indicates that the C3 controller exhibits a maximum tracking error of 26.41 N. The control accuracy of C2 (without prescribed performance) is significantly improved, with the maximum tracking error reduced to 18.13 N, which stabilizes below 12 N after 10 ms, validating the effectiveness of model compensation. The C1 controller further reduces the maximum tracking error to 1.98 N by adjusting the prescribed performance bounds (PP Boundary). Moreover, its tracking error can converge to the prescribed performance steady-state domain within the specified time T_{f}, whereas the errors of both C3 and C2 exceed these bounds. This verifies the effectiveness of the adopted finite-time prescribed performance control technique. The actual control input and desired valve position is shown in Figure 5.

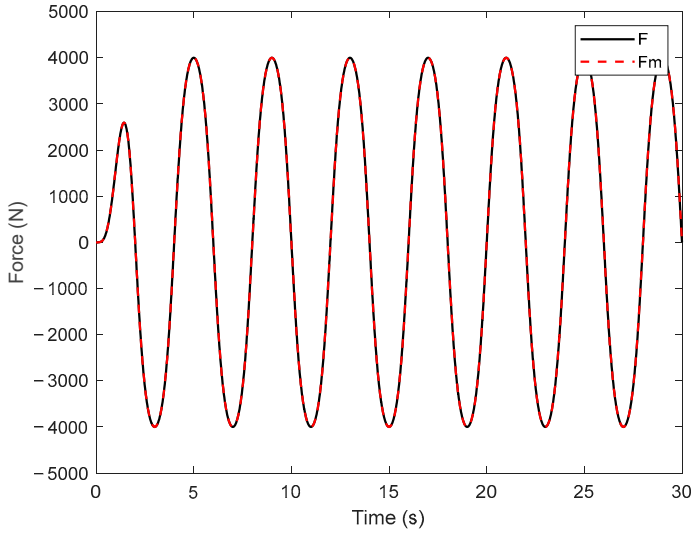


Figure 3. The desired trajectory and output of C1.

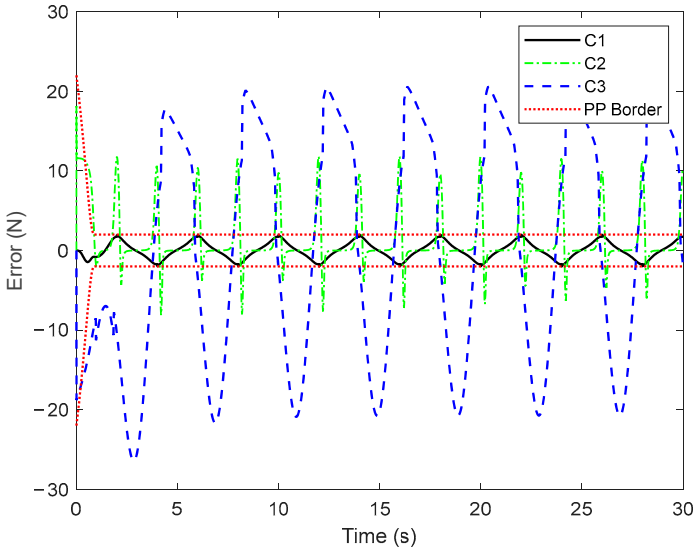


Figure 4. Tracking errors of the three compared controllers.

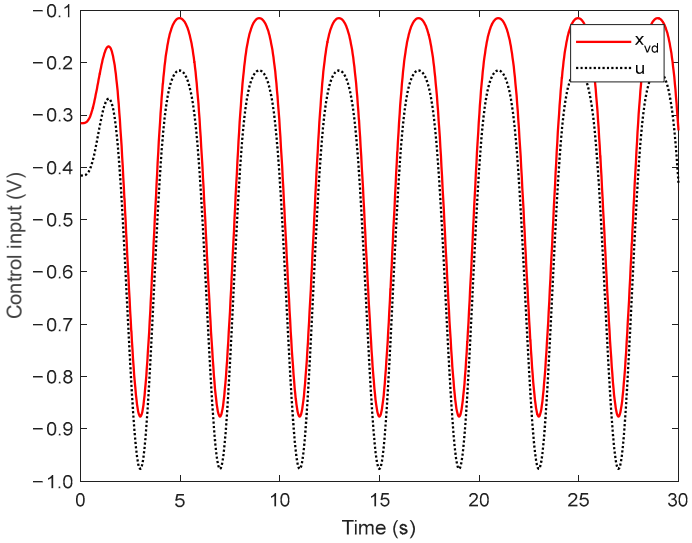


Figure 5. The actual control input and desired valve position of C1.

4.2. Case 2

The desired trajectory is selected as a point-to-point command with an amplitude of 4000 N, a maximum force change rate of 10 N/s, and a maximum force change acceleration of 40 N/s^2. The initial system force is set to 0 N. The simulation duration is 30 s with a step size of 0.2 ms.

The tracking performance of C3 is shown in Figure 6. The error comparison among all controllers is presented in Figure 7. Analysis shows that the C1 controller has a maximum tracking error of 18.79 N. The control accuracy of C2 is improved, with its maximum tracking error reduced to 18.13 N, stabilizing below 11 N after 10ms, again confirming the validity of model compensation. The C1 controller reduces the maximum tracking error to 7.27 N. Furthermore, after converging to the steady-state domain within the specified time T_f, the error stabilizes below 1 N for time t > T_f and consistently remains within the prescribed performance bounds. The errors of C3 and C2 controllers exceed these bounds, demonstrating the efficacy of the proposed finite-time prescribed performance control. The actual control input and valve position is shown in Figure 8.

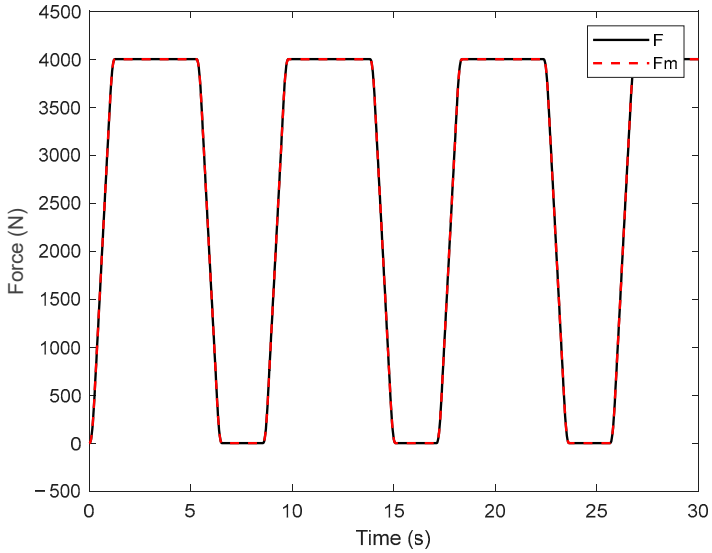


Figure 6. The desired trajectory and output of C1.

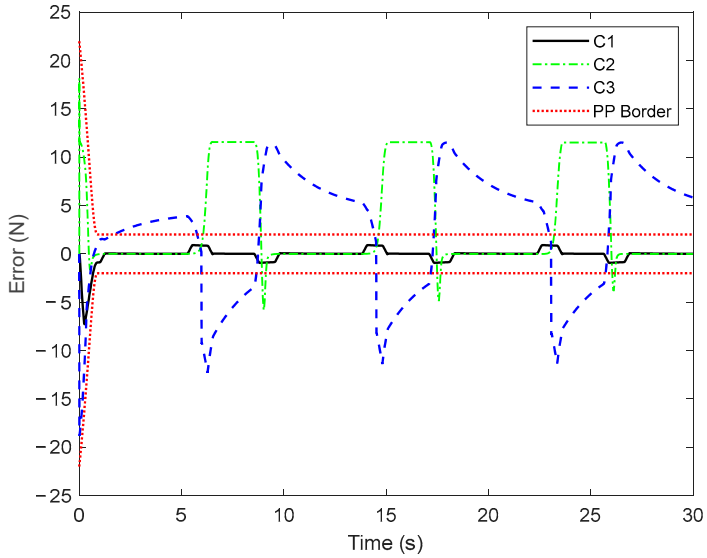


Figure 7. Tracking errors of the three compared controllers.

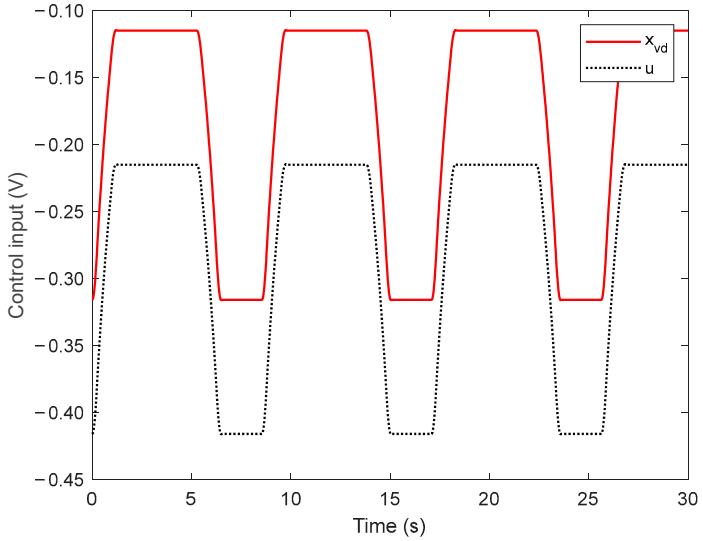


Figure 8. The actual control input and desired valve position of C1.

The results verify that the proposed control strategy C1 achieves the highest control accuracy. When tracking the sine-like trajectory, the maximum tracking error after T_f seconds is 0.0495% of the command amplitude. Compared to the C3 controller and the C2 controller (without prescribed performance), the control accuracy is improved by 92.5% and 83.5%, respectively. For the point-to-point trajectory, the maximum tracking error after T_f is 0.0025% of the command amplitude, representing accuracy improvements of 94.6% and 90.9% over the C3 and C2 controllers, respectively. Moreover, the tracking error is always confined within a bound after a pre-specified time.

5. Conclusions

This research concludes that the proposed prescribed performance output-feedback static loading control strategy offers distinct advantages for the electro-hydraulic proportional load simulator. It significantly enhances control precision, evidenced by reducing the maximum tracking error by over 92.5% and 83.5% for sinusoidal and point-to-point trajectories, respectively, compared to PI and model-based adaptive robust controller. This dramatic improvement is directly attributable to the core synthesis of two elements: The finite-time prescribed performance design and dead-zone compensation, and the former governs transient and steady-state error bounds by transforming constrained error, guaranteeing convergence into a predefined region within a preset finite time. These attributes make the strategy a robust solution for high-accuracy loading control. Furthermore, the strategy's output-feedback nature enhances its practical viability by reducing reliance on full-state measurement. Future research will focus on validating the algorithm under more extreme physical conditions and extending its application to domains such as material testing.

Author Contributions: Z.D.: conceptualization, methodology, writing—reviewing and editing, funding acquisition, supervision. C.L.: methodology, software, formal analysis, data curation. P.Z.: writing—original draft, validation, visualization. Y.J.: writing—original draft, visualization. J.Y.: funding acquisition, methodology. L.L.: validation, visualization. All authors have read and agreed to the published version of the manuscript.

Funding: This work was supported in part by the National Natural Science Foundation of China [Grant No. 52305056, 52075262], in part by Henan Province Science and Technology Research Project [Grant No. 242103810050].

Institutional Review Board Statement: Not applicable.

Informed Consent Statement: Not applicable.

Data Availability Statement: Data sets generated during the current study are available from the corresponding author on reasonable request.

Acknowledgments: We are grateful to the reviewers for sparing their time and efforts to manage this manuscript.

Conflicts of Interest: We declare that we have no financial and personal relationships with other people or organizations that can inappropriately influence our work, there is no professional or other personal interest of any nature in any product, service and/or company that could be construed as influencing the position presented in, or the review of, the manuscript entitled.

Appendix A

Defining a Lyapunov function as

$$V = \frac{\theta_1}{2}\log\frac{1}{1-\xi^2} + \frac{1}{2}\widetilde{\theta}^{\mathrm{T}}\Gamma_\theta^{-1}\widetilde{\theta} + \frac{1}{2}\widetilde{\vartheta}^{\mathrm{T}}\Gamma_\vartheta^{-1}\widetilde{\vartheta} + \frac{1}{2}\widetilde{W}^{\mathrm{T}}\Gamma_W^{-1}\widetilde{W} \tag{A1}$$

Taking the derivative of Equation (A1), and substituting Equations (23) and (26), ones have

$$\begin{aligned}\dot{V} &\le -\frac{k\xi^2}{\phi(1-\xi^2)} + \frac{\widetilde{\vartheta}^{\mathrm{T}}\widehat{\eta}g + \widetilde{\theta}_1\varphi - \widetilde{W}^{\mathrm{T}}\sigma(X)}{\phi(1-\xi^2)} + \frac{\xi(\widetilde{f}-\omega^*)}{\phi(1-\xi^2)} - \frac{\xi^2}{\phi^2(1-\xi^2)^2} + \widetilde{\theta}^{\mathrm{T}}\Gamma_\theta^{-1}\dot{\hat{\theta}} + \widetilde{\vartheta}^{\mathrm{T}}\Gamma_\vartheta^{-1}\dot{\hat{\vartheta}} + \widetilde{W}^{\mathrm{T}}\Gamma_W^{-1}\dot{\hat{W}} \\ &= -\frac{k\xi^2}{\phi(1-\xi^2)} + \frac{\xi(\widetilde{f}-\omega^*)}{\phi(1-\xi^2)} + \widetilde{\theta}^{\mathrm{T}}k_\theta\hat{\theta} + \widetilde{\vartheta}^{\mathrm{T}}k_\vartheta\hat{\vartheta} + \widetilde{W}^{\mathrm{T}}k_W\hat{W}\end{aligned} \tag{A2}$$

As $\log\frac{L^2}{L^2-z^2} < \frac{L^2}{L^2-z^2}$ in the interval $|z| < L$ [21], then setting $L = 1$, we have

$$\dot{V} \le -\frac{k}{\phi}\log\frac{1}{1-\xi^2} + \frac{\xi(\widetilde{f}-\omega^*)}{\phi(1-\xi^2)} - \frac{\xi^2}{\phi^2(1-\xi^2)^2} - \widetilde{\theta}^{\mathrm{T}}k_\theta\hat{\theta} - \widetilde{\vartheta}^{\mathrm{T}}k_\vartheta\hat{\vartheta} - \widetilde{W}^{\mathrm{T}}k_W\hat{W} \tag{A3}$$

Denoting υ as the upper bound of $\widetilde{f} - \omega^*$, and using Young Inequality,

$$\begin{aligned}&z_2 d_1 \le \tfrac{1}{2}z_2^2 + \tfrac{1}{2}\bar{d}_1^2\,, \quad z_2\delta_1^* \le \tfrac{1}{2}z_2^2 + \tfrac{1}{2}\delta_1^{*2}\,, \quad z_3\delta_2^* \le \tfrac{1}{2}z_3^2 + \tfrac{1}{2}\delta_2^{*2} \\ &\tfrac{\xi(\widetilde{f}-\omega^*)}{\phi(1-\xi^2)} \le \tfrac{\xi^2}{\phi^2(1-\xi^2)^2} + \tfrac{\upsilon^2}{4}\end{aligned} \tag{A4}$$

and the following property,

$$-\widetilde{W}^{\mathrm{T}}k_W\hat{W}_1 \le \frac{k_W}{2}(\|W\|^2 - \left\|\widetilde{W}\right\|^2)\,, \quad -\widetilde{\theta}^{\mathrm{T}}k_\theta\hat{\theta} \le \frac{k_\theta}{2}(\|\theta\|^2 - \left\|\widetilde{\theta}\right\|^2)\,, \quad -\widetilde{\vartheta}^{\mathrm{T}}k_\vartheta\hat{\vartheta} \le \frac{k_\vartheta}{2}(\|\vartheta\|^2 - \left\|\widetilde{\vartheta}\right\|^2) \tag{A5}$$

We can arrive at

$$\begin{aligned}\dot{V} &\le -\tfrac{k}{\phi}\log\tfrac{1}{1-\xi^2} - \tfrac{k_W}{2}\left\|\widetilde{W}\right\|^2 - \tfrac{k_\theta}{2}\left\|\widetilde{\theta}\right\|^2 - \tfrac{k_\vartheta}{2}\left\|\widetilde{\vartheta}\right\|^2 + \tfrac{1}{2}\bar{d}_1^2 + \tfrac{1}{2}\delta_1^{*2} + \tfrac{1}{2}\delta_2^{*2} + \tfrac{k_W}{2}\|W\|^2 + \tfrac{k_\theta}{2}\|\theta\|^2 + \tfrac{k_\vartheta}{2}\left\|\widetilde{\vartheta}\right\|^2 + \tfrac{\varepsilon^2}{4} \\ &\le -\kappa V + \Delta\end{aligned} \tag{A6}$$

Then we have

$$V \le V(0)e^{-\kappa t} + \frac{\Delta}{\kappa}(1 - e^{-\kappa t}) \tag{A7}$$

where $\kappa = \min\{2\theta_1 kP^{-1}, k_W/\eta(\Gamma_W{}^{-1}), k_\theta/\eta(\Gamma_\theta{}^{-1}), k_\vartheta/\eta(\Gamma_\vartheta{}^{-1})\}$, $\eta(\Gamma_W{}^{-1})$, $\eta(\Gamma_\theta{}^{-1})$ and $\eta(\Gamma_\vartheta{}^{-1})$ denote the minimum eigenvalues of $\Gamma_W{}^{-1}$, $\Gamma_\vartheta{}^{-1}$ and $\Gamma_\vartheta{}^{-1}$ respectively, $\Delta = (\bar{d}_1^2 + \delta_1^{*2} + \delta_2^{*2} + k_W\|W\|^2 + k_\theta\|\theta\|^2 + k_\vartheta\left\|\widetilde{\vartheta}\right\|^2 + 0.5\upsilon^2)/2$.

Thus, $V \in L_\infty$, the signal $\widetilde{\theta}, \widetilde{\vartheta}, \widetilde{W}$ are bounded, and $|\xi| < 1$, hence the tracking error z can meet the finite-time prescribed performance defined in Equations (15) and (16),

and $\hat{\theta}, \hat{\vartheta}, \hat{W}$ are also bounded. From Equations (20), (22) and (24), the desired valve spool displacement x_{vd} and control input u are bounded. Thus, the proof is completed.

References

1. Yao, J.; Jiao, Z.; Yao, B.; Dong, W. Nonlinear adaptive robust force control of hydraulic load simulator. *Chin. J. Aeronaut.* **2012**, *25*, 766–775. [CrossRef]
2. Li, J.; Li, W.; Liang, H.; Kong, L. A review of the research on electro-hydraulic load simulator and characteristics with improvement methods. *Recent Pat. Eng.* **2024**, *18*, 45–56. [CrossRef]
3. Hao, H.; Yan, H.; Zhang, Q.; Li, H. Pressure Control of Multi-Mode Variable Structure Electro–Hydraulic Load Simulation System. *Sensors* **2024**, *24*, 7400. [CrossRef] [PubMed]
4. Stosiak, M.; Karpenko, M. The influence of the hydropneumatic accumulator on the dynamic and noise of the hydrostatic drive operation. *Eksploat. Niezawodn.-Maint. Reliab.* **2024**, *26*, 186169. [CrossRef]
5. Mohanty, A.; Yao, B. Indirect adaptive robust control of hydraulic manipulators with accurate parameter estimates. *IEEE Trans. Control Syst. Technol.* **2010**, *19*, 567–575. [CrossRef]
6. Wu, Z.; Gao, Z.; Chen, Y.; Liu, Y. On transitioning from PID to ADRC in thermal power plants. *Control Theory Technol.* **2021**, *19*, 3–18. [CrossRef]
7. Fischer, N.; Kan, Z.; Kamalapurkar, R.; Dixon, W.E. Saturated RISE feedback control for a class of second-order nonlinear systems. *IEEE Trans. Autom. Control* **2013**, *59*, 1094–1099. [CrossRef]
8. Dong, Z.; Bai, D.; Zhang, P.; Yao, J. Prescribed Performance Adaptive Neural Network Tracking Control of Electro-hydraulic Servo System with Input Delay. *Appl. Math. Model.* **2025**, *152*, 116591. [CrossRef]
9. Nguyen, T.T.; Otieno, L.O.; Nguyen, T.N. Nonlinear Modeling of a Piezoelectric Actuator-Driven High-Speed Atomic Force Microscope Scanner Using a Variant DenseNet-Type Neural Network. *Actuators* **2024**, *13*, 391. [CrossRef]
10. Yao, J.; Jiao, Z.; Ma, D. High dynamic adaptive robust control of load emulator with output feedback signal. *J. Frankl. Inst.* **2014**, *351*, 4415–4433. [CrossRef]
11. Zhang, Z.; Park, J.H.; Zhang, K.; Lu, J. Adaptive control for a class of nonlinear time-delay systems with dead-zone input. *J. Frankl. Inst.* **2016**, *353*, 4400–4421. [CrossRef]
12. Zong, G.; Wang, Y.; Karimi, H.R.; Shi, K. Observer-based adaptive neural tracking control for a class of nonlinear systems with pre scribed performance and input dead-zone constraints. *Neural Netw.* **2022**, *147*, 126–135. [CrossRef] [PubMed]
13. Tao, G.; Kokotovic, P.V. Adaptive control of plants with unknown dead-zones. *IEEE Trans. Autom. Control* **1994**, *39*, 59–68.
14. Zhou, J.; Wen, C.; Zhang, Y. Adaptive output control of nonlinear systems with uncertain dead-zone nonlinearity. *IEEE Trans. Autom. Control* **2006**, *51*, 504–511. [CrossRef]
15. Deng, W.; Yao, J.; Ma, D. Robust adaptive precision motion control of hydraulic actuators with valve dead-zone compensation. *ISA Trans.* **2017**, *70*, 269–278. [CrossRef]
16. Dong, Z.; Duan, Y.; Bai, D.; Zhang, P.; Yao, J.; Sun, H. Prescribed performance asymptotic tracking control for disturbed nonlinear system with uncertain dead-zone. *Proc. Inst. Mech. Eng. Part I J. Syst. Control Eng.* **2025**, *239*, 1439–1451. [CrossRef]
17. Bechlioulis, C.P.; Rovithakis, G.A. Robust adaptive control of feedback linearizable MIMO nonlinear systems with prescribed performance. *IEEE Trans. Autom. Control* **2008**, *53*, 2090–2099. [CrossRef]
18. Qiu, J.; Wang, T.; Sun, K.; Rudas, I.J.; Gao, H. Disturbance observer-based adaptive fuzzy control for strict-feedback nonlinear systems with finite-time pre scribed performance. *IEEE Trans. Fuzzy Syst.* **2021**, *30*, 1175–1184. [CrossRef]
19. Yao, Y.; Kang, Y.; Zhao, Y.; Li, P.; Tan, J. Flexible prescribed performance output feedback control for nonlinear systems with input saturation. *IEEE Trans. Fuzzy Syst.* **2024**, *32*, 6012–6022. [CrossRef]
20. Wang, H.; Bai, W.; Zhao, X.; Liu, P.X. Finite-time-prescribed performance-based adaptive fuzzy control for strict-feedback nonlinear systems with dynamic uncertainty and actuator faults. *IEEE Trans. Cybern.* **2021**, *52*, 6959–6971. [CrossRef]
21. Zhou, T.; Liu, C.; Liu, X.; Wang, H.; Zhou, Y. Finite-time prescribed performance adaptive fuzzy control for unknown nonlinear systems. *Fuzzy Sets Syst.* **2021**, *402*, 16–34. [CrossRef]

Disclaimer/Publisher's Note: The statements, opinions and data contained in all publications are solely those of the individual author(s) and contributor(s) and not of MDPI and/or the editor(s). MDPI and/or the editor(s) disclaim responsibility for any injury to people or property resulting from any ideas, methods, instructions or products referred to in the content.